CONF-951155--97

NANOCRYSTAL FORMATION VIA YTTRIUM ION IMPLANTATION INTO SAPPHIRE

E. M. HUNT *, J. M. HAMPIKIAN *, D. B. POKER **
*School of Materials Science and Engineering, Georgia Institute of Technology, 778 Atlantic Dr. Atlanta Georgia, 30332-0245
** Solid State Division, Oak Ridge National Laboratory, Oak Ridge, TN 37831

ABSTRACT

Ion implantation has been used to form nanocrystals in the near surface of single crystal α-Al_2O_3. The ion fluence was 5 x 10^{16} Y^+/cm^2, and the implant energies investigated were 100, 150, and 170 keV. The morphology of the implanted region was investigated using transmission electron microscopy, x-ray energy dispersive spectroscopy, Rutherford backscattering spectroscopy and ion channeling. The implantation causes the formation of an amorphous surface layer which contains spherical nanosized crystals with a diameter of ~13 nm. The nanocrystals are randomly oriented and exhibit a face-centered cubic structure with a lattice parameter of ~4.1 A ± .02 A. Preliminary chemical analysis shows that these nanocrystals are rich in aluminum and yttrium and poor in oxygen relative to the amorphous matrix.

INTRODUCTION

Ion implantation has long been used as a means to alter the surface mechanical properties of metals (increased wear and corrosion resistance) and ceramics (improved toughness). It has more recently been established that ion implantation can alter the optical properties of ceramic materials. In particular, a picosecond non-linear response and surface plasmon resonances can be obtained from both Au and Cu ion-implanted fused silica and Au and Ag ion-implanted alumina,[1,2] and other systems. [3,4] The non-linear response is due to the formation of colloidal nanocrystals with particle sizes on the order of 10 nm and smaller.

Such particles can also be made in glasses using standard, but carefully controlled glass forming techniques. [5,6,7] However, the formation of these particles using ion implantation has several advantages, [1,8] including control of the amount and purity of the implanted species, a higher density of particles, and control of the depth of the implant which allows formation of thin layers of particles at specific depths, rather than the random particle placement throughout the bulk material that results from melt processing. Metallic colloids have been formed in alumina as a result of ion implantation of Fe,[9] Au,[10] and Ni.[11,12] In this paper, we report the synthesis of colloidal nanoclusters which form within amorphous alumina as a result of yttrium ion implantation into single crystal α-Al_2O_3

EXPERIMENTAL

Single crystal, high purity sapphire substrates, 1cm x 1cm x 0.07 cm were annealed at 1500 °C for 80 hours to remove residual polishing damage prior to ion implantation. Singly

charged yttrium ions (Y^+) with accelerating potentials of 100, 150 or 170 keV were implanted into the sapphire substrates to a total fluence of $5x10^{16}$ Y^+/cm^2 at a dose rate of ~ 3.3μA cm^{-2}, the pressure during implantation being ≈ $5x10^{-6}$ Pa. Samples were implanted at ambient temperature, while affixed to water cooled copper blocks with conductive paint. The surfaces of all of the implanted substrates became golden in color as a result of the implantation.

As-implanted substrates were characterized using 1.5 MeV Rutherford backscattering spectroscopy (RBS), and ion channeling (RBS-C). Knoop microhardness measurements were obtained using a Lecco DM-400 hardness tester in accordance with the ASTM standard for microhardness testing E 384-89. The hardness of each substrate was sampled as a function of depth by making indentations with a series of seven loads ranging from 10 grams to 500 grams and determining hardness numbers for those indents. These hardness values were then normalized by dividing them by similarly obtained hardness values from the unimplanted side of the same specimen.

Transmission electron microscopy (TEM) and energy dispersive x-ray spectroscopy (EDS) were carried out using a Hitachi HF-2000 field emission gun transmission electron microscope with digital acquisition capability operated at 200 keV. Plan-view TEM samples were prepared by mechanically thinning the specimens followed by argon ion sputtering at liquid nitrogen temperatures. The ion mill employed a low current (~1 mA), 5 keV beam of argon ions which was positioned at an angle of approximately 12-14 degrees from the sample surface.

RESULTS

Rutherford Backscattering Spectroscopy and Ion Channeling

RBS and RBS-C results show that yttrium ion implantation at 100, 150, and 170 keV resulted in the formation of a non-channeling surface layer such as would be caused by the presence of amorphous or heavily damaged material. The channeling and non-channeling spectra for the 150 keV implanted substrate are representative of all three implant energies and are presented in Figure 1. The thickness of the damaged layer may be calculated by measuring the full width of the non-channeling layer and equating it with depth through the use of a depth calibration based on the stopping power of alumina. This conversion yields thicknesses of 86 nm ± 4 nm, 119 nm ± 6 nm, and 121 nm ± 6 nm for 100, 150, and 170 keV, respectively. This result is as expected; the higher energy yttrium ions penetrate further, imparting more energy to the surrounding substrate material, thereby causing a larger non-channeling region.

The yttrium peaks from the non-channeling spectra of the as-implanted samples are shown in Figure 2. For increasing implanted ion energies the peak of the implant lies at successively lower energies, which corresponds to greater depths beneath the surface. The absolute depth of the yttrium peak cannot be determined from this data because of sample charging effects due to the use of a singly charged beam for RBS analysis. The charging effect in a case such as this is typically small in comparison to the width of the peak (a 2-3 channel shift of a peak many channels wide) so the change in location as a function of implant energy can be estimated after alligning the Al edges of the three spectra. The depth increases with respect to the 100 keV spectra for both of the higher energy spectra; the 150 keV Y peak is 250 nm deeper and the 170 keV peak is 362 nm deeper. The FWHM of the implant peak also increases with implant energy, as expected.

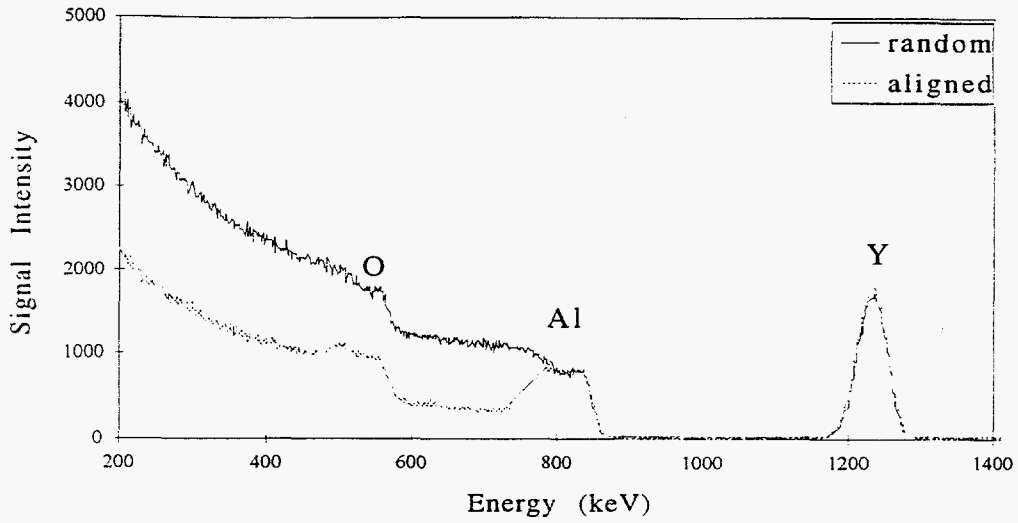

Figure 1: RBS Spectra for the 150 keV as-implanted sample.

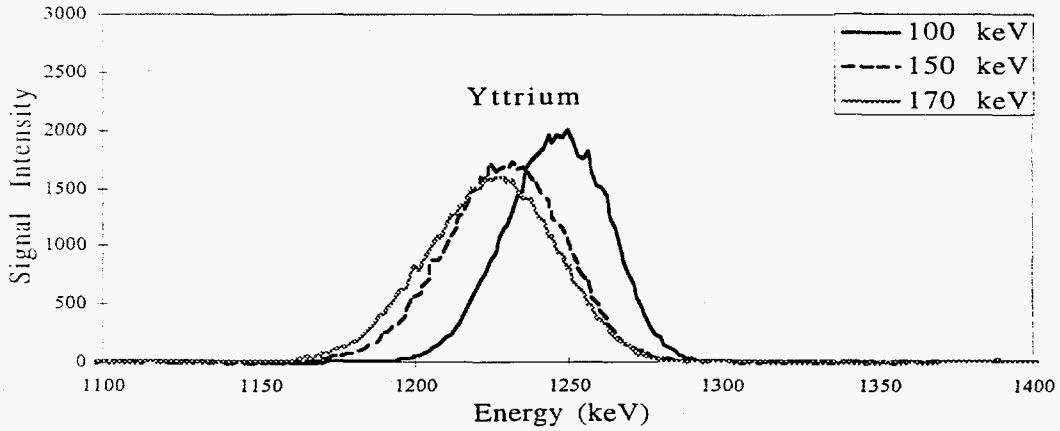

Figure 2: RBS Yttrium peaks for the three implant energies.

Knoop Hardness Measurements

The hardness values obtained for the 100 keV, 150 keV and 170 keV as-implanted surfaces indicate that the implantation in each case has not merely damaged the surface, but has fully amorphized the surface. Figure 3 is a plot of load versus normalized hardness for both of these samples. It can be seen that the implanted surface is much softer than the unimplanted surface, as indicated by the low load normalized harness values being much less than one. With increasing depth (increasing load) the hardness of the implanted surface approaches that of the virgin substrate. Burnett and Page[13] have shown that, in alumina, absolute softening (treated surface being softer than the untreated surface) occurs when a surface amorphous layer is formed by implantation damage.

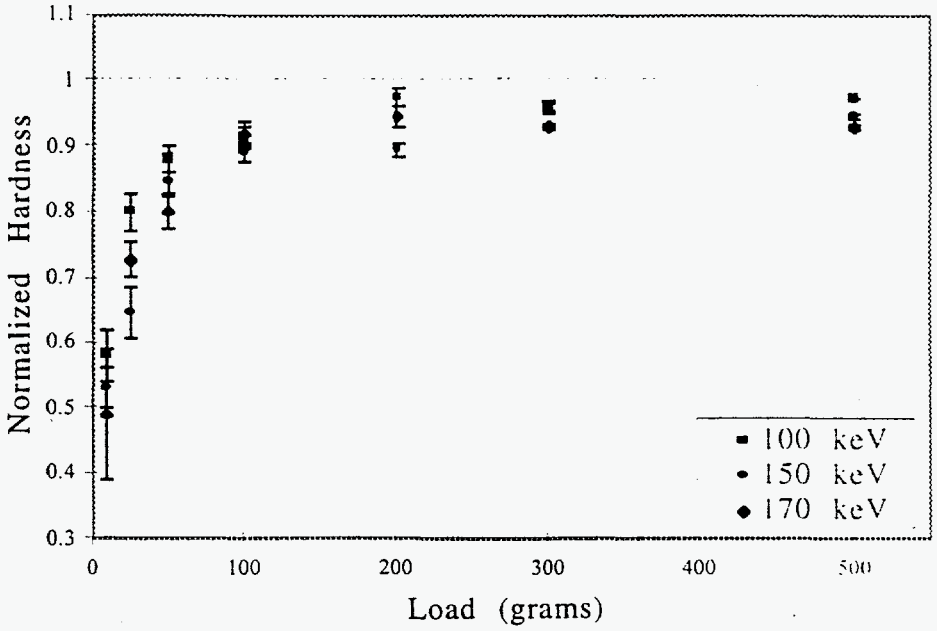

Figure 3: Normalized Knoop hardness values for the as-implanted substrates.

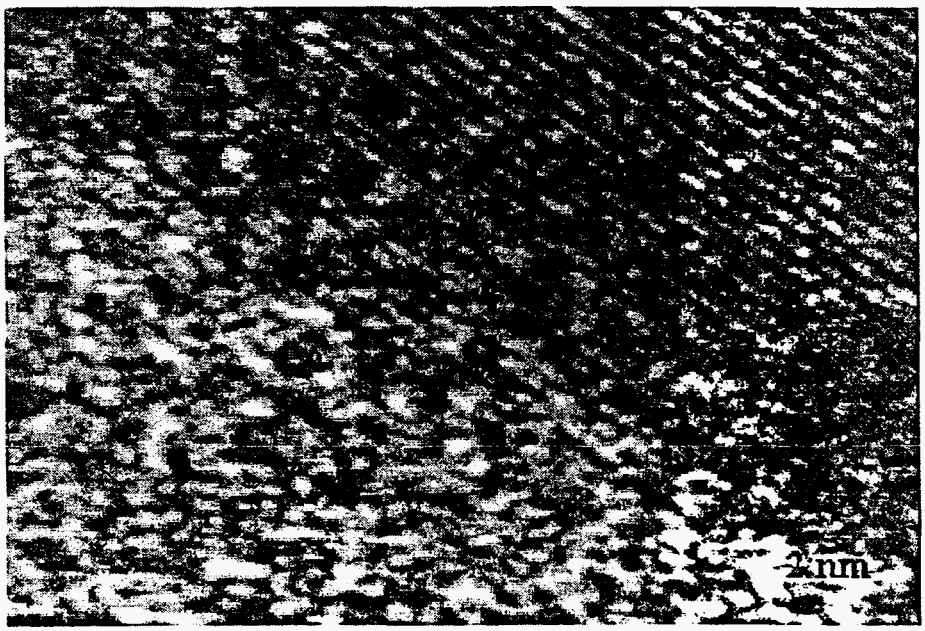

Figure 4: Bright field image of the amorphous surface region of an implanted substrate (lower left), and crystalline α-Al_2O_3 (upper right).

Transmission Electron Microscopy

Examination of the as-implanted samples in cross-section by TEM confirms that the sample surfaces were rendered amorphous by the implantation treatment. Figure 4 presents an image which was taken from a cross sectional sample in an area near the surface of the substrate implanted at 150 keV. This micrograph was obtained from a region on the sample which showed the amorphous/crystalline transition region. Thus the lower represents contrast typical of amorphous material and the upper right displays lattice fringes from the crystalline alumina. Similar contrast and lack of lattice fringes were seen in the samples implanted at other energies.

Plan view specimens of the 150 and 170 keV as-implanted substrates reveal nanosized particles embedded in the amorphous matrix material. These particles range in size from 12.5 nm ± 0.3 nm to 13.6 nm ± 0.8 nm. Figure 5 shows bright and dark field TEM images from areas containing particles from both the 150 keV and 170 keV plan view samples. Diffraction patterns from these areas exhibit a polycrystalline ring pattern arranged in a characteristic face-centered cubic pattern, see inset in Figure 5.

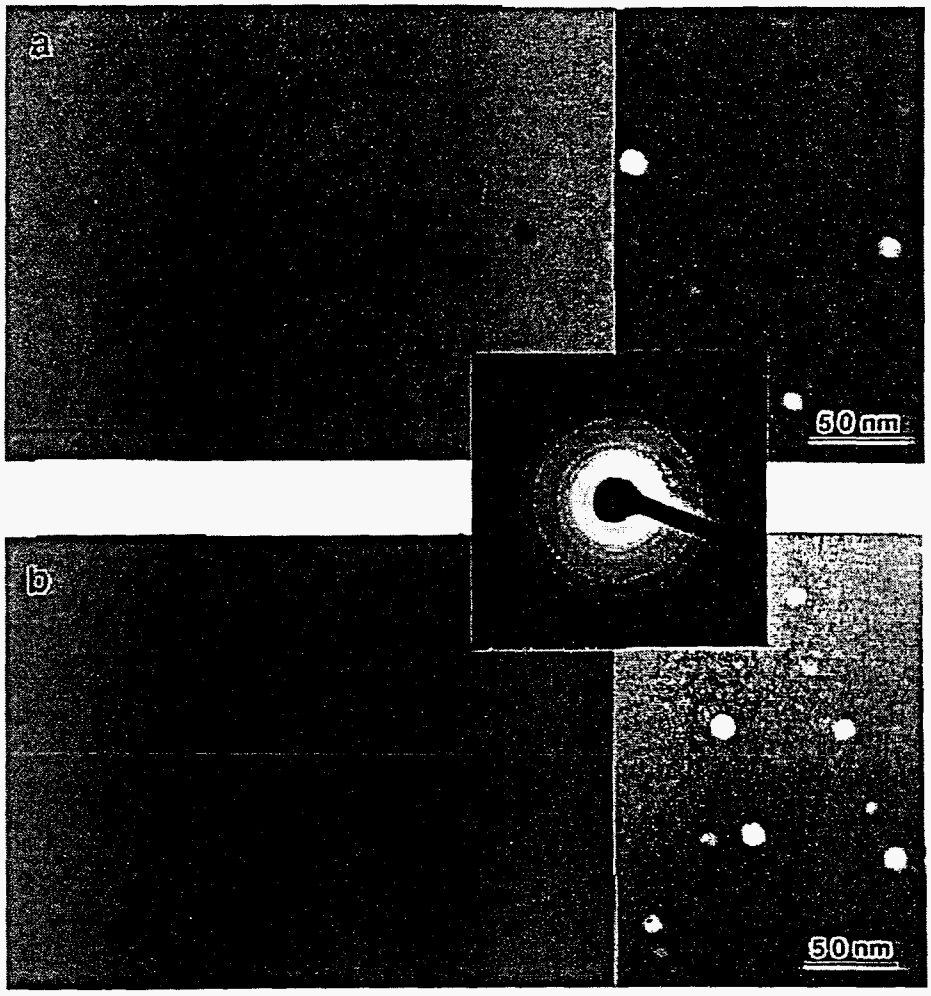

Figure 5: Bright and dark field TEM images of the 150 and 170 keV micro-structures which contain FCC particles with an average diameter of 12-13 nm.

The presence of rings indicates that these particles are not preferentially oriented, which is a reasonable finding, considering that they reside in an amorphous matrix. Upon calibration of the microscope's electron optics with a gold calibration standard, a lattice parameter of 0.412 nm ± 0.002 nm was calculated from these rings.

A high resolution digital image of a [110] oriented particle (see Figure 6) allowed an independent calculation of the lattice parameter for this material. Using measurements from the fast Fourier transform in Figure 6 a lattice parameter of 0.411 nm ± 0.003 nm was obtained, after calibration with a lattice image of Au taken with the same CCD camera. This lattice parameter agrees well with that calculated from the polycrystalline diffraction pattern in Figure 5.

These particles were seen most easily in the plan view samples; however, dark field imaging did show particle-like structures of the appropriate size in one cross-sectional sample. In addition, the diffraction pattern associated with the particles was seen in two other cross-sectional samples. The particles' lack of visibility in most cross-sectional samples can be attributed to the difficulty in obtaining electron transparent areas which span the entire implanted depth. In plan view, the particles are not found in the areas immediately adjacent to the "hole", which implies that they are buried to some extent beneath the substrate surface. Thus the cross-sections, which have thin area only at the substrate surface, would not appear to contain particles. Other researchers have had similar difficulty observing particles in cross-sectional samples.[6]

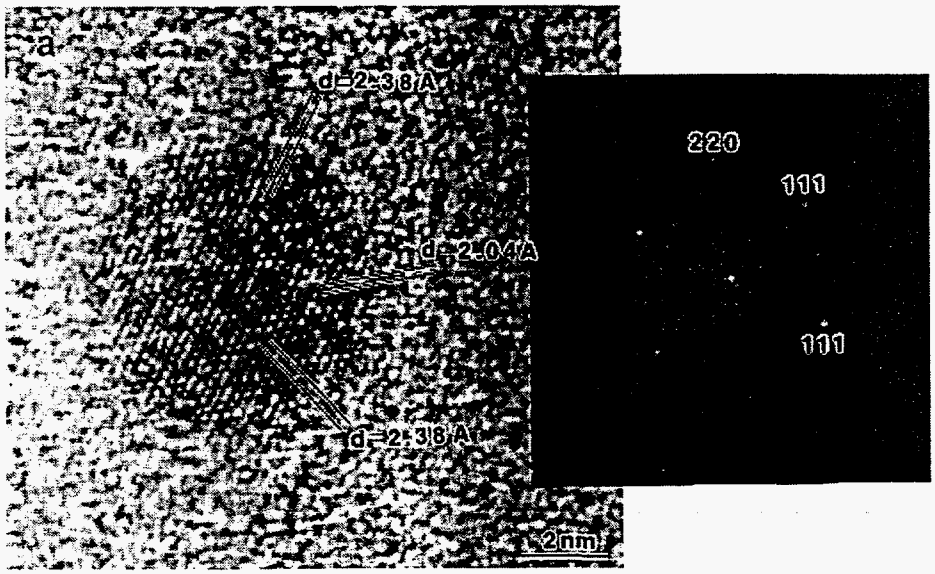

Figure 6: Digitally acquired high resolution image of a (110) oriented particle and the fast Fourier transform used in the calculation of a lattice parameter of 0.411A.

CONCLUSIONS

Implantation of yttrium ions into sapphire substrates to a fluence of $5x10^{16}$ Y^+/cm^2 at energies of 150 and 170 keV results in the formation of a surface amorphous layer containing nano-scale metallic particles with a lattice parameter of approximately 0.412 nm. This value is

just slightly larger than the lattice parameter of FCC aluminum (0.401 nm). The large size of the yttrium atoms and the resemblance of these particles to pure aluminum in both structure and lattice parameter lead to the hypothesis that the particles are a yttrium-aluminum metastable alloy. There are no stable Al-Y alloys that display a face centered cubic structure, nor is there any evidence in the diffraction data that indicates hexagonal symmetry, such as that displayed by pure yttrium. Chemical analysis and optical properties testing to confirm this conclusion are underway.

ACKNOWLEDGMENTS

This research was sponsored by the U.S. Department of Energy under contract # DE-AC05-96OR 22464 with Lockheed Martin Energy Research Corporation. We gratefully acknowledge the financial support of the Engineering Foundation and the Molecular Design Institute. We also thank Professors Z. L. Wang and J. Cochran Jr., and Ms.Yolande Berta for their assistance.

REFERENCES

1 Ch. Buchal, S. P. Withrow, C. W. White, D. B. Poker, Annu. Rev. Mater. Sci., **24**, 125-157, 1994.

2 R. F. Haglund, Jr., L.Yang, R. H. Macgruder III, J. E. Wittig, K. Becker, R. A. Zuhr, Optics Lett., **18**, (5), 373-375, 1993.

3 Z. L. Wang, J. M. Cowley, Ultramicroscopy, **21**, 77-94, 1987.

4 A. P. Mouritz, D. K. Sood, D. H. St John, M. V. Swain, J. S. Williams, Nuc. Inst. & Meth. B, **B19/20**, 805-808, 1987.

5 J. Allegre, G. Arnaud, H. Mathieu, P. Lefebvre, W. Granier, L. Bondes, J. Cryst. Growth., **138**, 998-1003,1994.

6 M. Allais, M Gandais, Mat. Sci. Eng., **B9**, 429-432, 1991.

7 R. H. Doremus, J. Chem. Phys., **40** (8), 2389-2396, 1986.

8 P. D. Townsend, Rep. Prog. Phys., **50**, 501-558, 1987.

9 P. S. Sklad, C. J. McHargue, C. W. White, G. C. Farlow, J. Mat. Sci., **27** (21), 5895-5904, 1992.

10 M. Ohkubo, N. Suzuki, Phil. Mag. Lett., **57** (5), 261-265, 1988.

11 G.C. Farlow, P.S. Sklad, C. W. White, C. J. McHargue, J. Mater. Res. **5** (7), 1502-1519, 1990.

12 M. Ohkubo, T. Hioki, J. Kawamoto, J. Appl. Phys., **60** (4), 1325-1335, 1986.

13 P. J. Burnett, T. F. Page, Rad. Eff., **97**, 283-296, 1986.